

UCLA

UCLA Electronic Theses and Dissertations

Title

Mechanical Design of a Cartesian Manipulator for Transducer Placement in Nondestructive Evaluation Experiments

Permalink

<https://escholarship.org/uc/item/58m2z27j>

Author

Zhang, Yichi

Publication Date

2020

Supplemental Material

<https://escholarship.org/uc/item/58m2z27j#supplemental>

Peer reviewed|Thesis/dissertation

UNIVERSITY OF CALIFORNIA

Los Angeles

Mechanical Design of a Cartesian Manipulator for Transducer Placement in Nondestructive
Evaluation Experiments

A thesis submitted in partial satisfaction
of the requirements for the degree Master of Science
in Mechanical Engineering

by

Yichi Zhang

2020

© Copyright by

Yichi Zhang

2020

ABSTRACT OF THE THESIS

Mechanical Design of a Cartesian Manipulator for Transducer Placement in Nondestructive Evaluation Experiments

by

Yichi Zhang

Master of Science in Mechanical Engineering

University of California, Los Angeles, 2020

Professor Ajit K. Mal, Chair

Nondestructive evaluation methods often require high accuracy of transducer placement and repetition of multiple experimental steps. This study proposes the design of a Cartesian manipulator robot to accurately move and place the transducers on the test specimen. The electrical and software systems are also developed to allow the automation of the experiment by creating a program. The robot is capable of linear speeds of 250 mm/s and the ranges of motion from 50 to 1000 mm with 0.05-mm position accuracy. The allowable workspace is 900 x 930 x 18 mm in dimensions (length x width x height) and the maximum load capacity is 25 kg. The software allows for 13 commands that can be combined freely in a variety of experiment settings. The manipulator will be used in the nondestructive evaluation of composite aircraft and aerospace structural components in Professor Mal's laboratory.

The thesis of Yichi Zhang is approved.

Dennis W. Hong

Chang-Jin Kim

Ajit K. Mal, Committee Chair

University of California, Los Angeles

2020

DEDICATION

I dedicate this work to my mother *Xiaokang Ji* and my father *Jian Zhang*.

感谢你们赐予我生命、物质，和一往无前的勇气。

TABLE OF CONTENTS

I.	Introduction	1
II.	Mechanical Design	4
1.	Linear Guides.....	4
2.	End-Effector Actuator and Housing	7
2.1.	CAD Design	8
2.2.	Finite-Element Analysis	13
2.3.	Driving Motor Selection.....	20
2.4.	Cam Profile Design	21
2.5.	Assembly of System.....	23
2.6.	Workspace of System	24
III.	Electrical Design.....	25
1.	Linear Guides.....	25
2.	Top Stepper Motor.....	26
IV.	Software Design.....	29
1.	Connect Controller (CNCT CTL).....	30
2.	Manual Operation (MNL OPER).....	30
3.	Set Parameters (Set PARM).....	32
4.	Edit Program (Edite PGM)	34
5.	Company and Laboratory Information (About).....	38
V.	Product Demonstration	39
VI.	Concluding Remarks.....	42
	References.....	43

LIST OF FIGURES

Figure 1. Gantry structure of a Cartesian manipulator	2
Figure 2. High-precision ball-screw linear motion guide from Fuyu Technology	5
Figure 3. Assembly of the linear guide system of four linear guides	6
Figure 4. Corner blocks for positioning linear guides perpendicularly and for stable ground support.....	6
Figure 5. Exploded view and assembled view of end-effector actuator and housing.....	8
Figure 6. CAD design of inner race	9
Figure 7. 2D sectional view of the end-effector actuator system	11
Figure 8. 2D sketch of the end-effector actuator system	12
Figure 9. Modified end-effector system for manual operation	13
Figure 10. Actuator housing in the static structural test	14
Figure 11. Summary of fixture features and loading conditions	16
Figure 12. Illustration of the housing mesh condition	17
Figure 13. FEA result with the color gradient depicting stress value at different locations.....	18
Figure 14. FEA result with the color gradient depicting displacement and strain value at different locations	18
Figure 15. FEA result with the color gradient depicting displacement and strain value at different locations	19
Figure 16. Illustration of the cam profile	22
Figure 17. Assembly of the Automated Grid System.....	23
Figure 18. Reachable workspace of the Automated Grid System (900 x 930 x 18 mm)	24
Figure 19. Wiring diagram of the linear guide system	25
Figure 20. Wiring diagram of the end-effector actuator system.....	27
Figure 21. Software layout: 1) language selection, 2) operation tabs, and 3) operation window. 29	
Figure 22. Manual Operation tab interface: 1) manual control panel and 2) machine status panel	32
Figure 23. Set Parameters tab interface	34
Figure 24. Edite Programs tab interface.....	35
Figure 25. List of available commands to preset the program.....	36
Figure 26. Example program: incremental movement of transducer	38
Figure 27. End-effector actuator system.....	39
Figure 28. Isometric view of final assembly.....	40
Figure 29. Top view of final assembly	40
Figure 30. Wiring of linear guide system	41
Figure 31. Wiring of end-effector actuator system.....	41

I. Introduction

Failure of aircraft and aerospace structural members can have fatal and disastrous repercussions, with the loss of lives and of the structure ^[2]. Therefore, inspection and study of defects in these members are of importance to reduce unexpected failure of the structures. Reliable, efficient and cost-effective non-destructive evaluation (NDE) techniques are needed ^[1] to detect the initiation and growth of hidden damage in defects-critical structures to assure their safety and integrity during service. Ultrasonic (UT) wave-based methods are widely used for the NDE of a variety of structures due to their low cost, ease of use and the ability to work on a multitude of material systems. However, in their current versions, the UT based techniques are extremely time consuming for testing large structures and dependent on bulk waves to be used effectively for complex materials (e.g., composite aircraft or rockets). A recent UT method based on guided lamb waves has the potential to significantly improve the state of ultrasonic NDE due to their ability to travel relatively large distances and their sensitivity to small defects inside structure. The development of such techniques requires experiment setups with optimal accuracy in the placement of transducers ^{[3][4][5]}. However, in a variety of experiments, manual alignment in experiments is still used. In this paper, we devise a planar robot system that provides high accuracy and speed, as well as the automation of experiments for the Material Degradation Laboratory at UCLA.

The planar robot system, termed “Automated Grid System (AGS)”, developed in this thesis, takes advantage of the Cartesian manipulator system. In the field of robotics, manipulation methods can be narrowed down to five: Cartesian, Cylindrical, SCARA, 6-Axis and Delta. Each industrial robot type has its characteristics that make it best-suited for certain applications. The

main differentiators are speed, size and workspace. For our application, the Cartesian Robotic Manipulator is selected. The linear movements of the Cartesian elements give the robot a cube-shaped workspace that fits well with pick-and-place applications in the scale several centimeters to meters. Cartesian Manipulators also provide good mechanical stiffness and operation speed with constant wrist-positioning accuracy in the entire workspace ^[6]. An example of Cartesian robotic manipulator is the Gantry structure shown in Figure 1 ^[7].

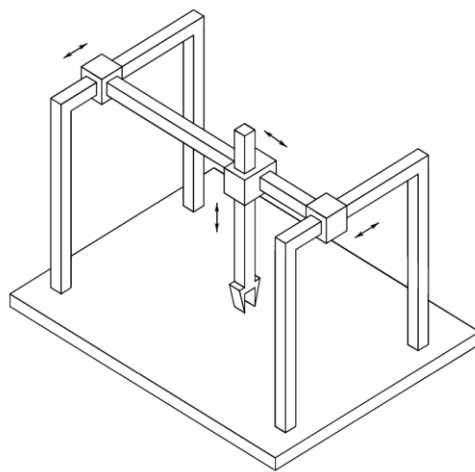


Figure 1. Gantry structure of a Cartesian manipulator ^[7]

The number of Degrees of Freedom (DOF) of a manipulator is the number of independent position variables required to locate all parts of the mechanism. To place and orient an object in the three-dimensional (3-D) space, six DOFs are needed—three for positioning a point on the object and three for orienting the object with respect to a reference coordinate frame ^[6]. In our study, a 3-DOF Cartesian manipulator is developed, so three spatial parameters are required and the orientation of the attached device is unchanged. The attached device, called the “end effector”, is attached at the end of the manipulator links for interaction with the environment or work object.

An end-effector can be a gripper, a welding torch, a probe or any other device ^[7]. In the case of nondestructive evaluation, it is often a transducer.

The novelty of this robot is three-fold. First, the incorporation of the end-effector actuator system allows the user to mount a high- or low-frequency transducer as the end effector and apply even pressure on the top surface for consistent force distribution. Second, the software design allows for complete automation after the user presets a program. Third, the high accuracy of transducer placement can improve the experimental setup of nondestructive evaluation and increase the capacity of locating the damage.

II. Mechanical Design

The mechanical components are of two categories: the linear guide system and the end-effector actuator system. The linear guide system allows the movement of the end effector in the x- and y-direction inside the work plane (parallel to the test plate) while the end-effector actuator system allows the movement in z-direction perpendicular to the work plane. The end effector, a high-frequency or low-frequency transducer depending on the experimental requirement, is first attached to the top connector. The top connector is then mounted onto the stage of the Cartesian manipulator. The Cartesian manipulator is capable of moving in a 2-D work plane, therefore carrying the transducer to the desired location. Once the transducer is at the experiment location, the top connector presses it down onto the specimen in test with a stepper motor to guarantee optimal contact. The components and work mechanism of each system are discussed below.

1. Linear Guides

The linear guide system consists of four high-precision ball-screw linear motion guides purchased from Fuyu Technology Inc ^[10]. The product is shown in Figure 2. During operation, the top stepper motor actuates the ball screw mechanism, which translates the rotational motion of the threaded rod into linear motion of the stage.

Table 1 is a summary of selected parameters. Please note that the maximum horizontal load is when the load is on top of the stage and the maximum vertical load is when the load is on the side of the stage.



Figure 2. High-precision ball-screw linear motion guide from Fuyu Technology ^[10]

Fuyu FTS40X100Y100-H1	
Position Accuracy	0.05 mm
Effective Stroke	50-1000 mm
Maximum Horizontal Load	25 kg
Maximum Vertical Load	1 kg
Maximum Speed	250 mm/s
Maximum Acceleration	200 mm/s ²
Noise	65 dB

Table 1. Summary of selected parameters of Fuyu linear guide ^[10]

When the four high-precision ball-screw linear motion guides are assembled as shown in Figure 3, one of the two stages (stage #1) can move in the x- and y-directions while the other (stage #2) can only move in the y-direction. Both stages can be connected to transducers for excitation and receiving operations. The corner blocks are designed and fabricated with 3-D printing. Please

note that the two corner blocks have different designs to accommodate the contour of the linear guide.

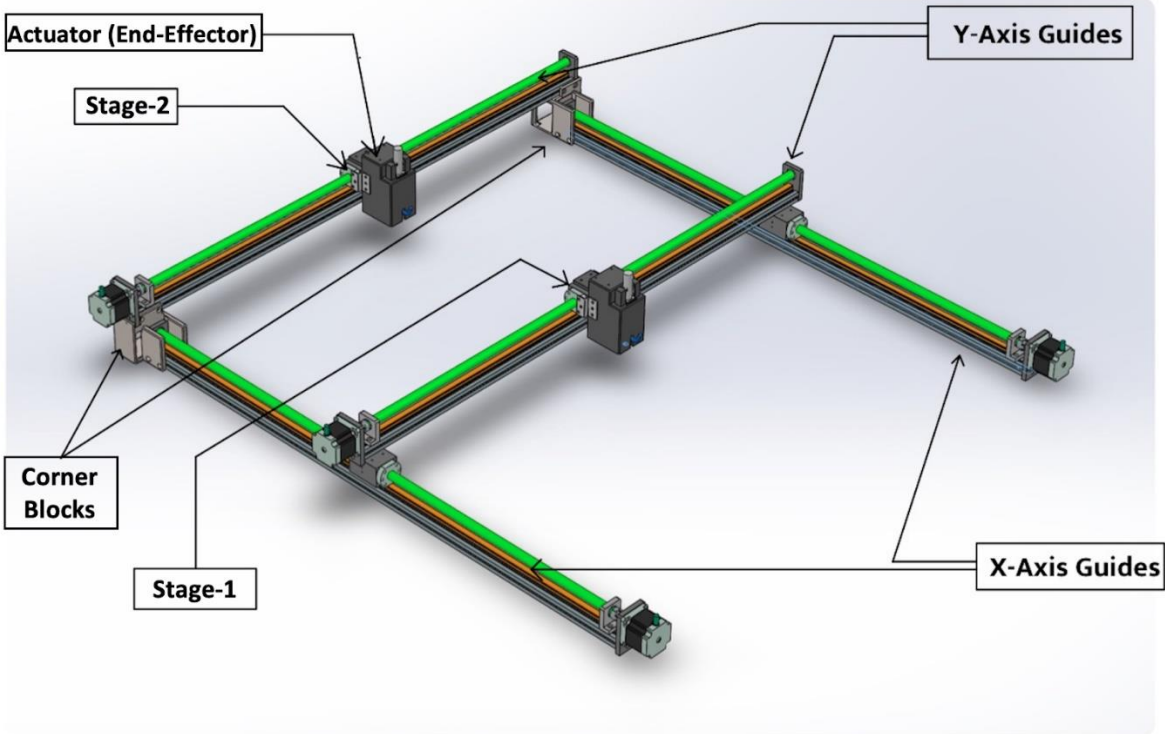


Figure 3. Assembly of the linear guide system of four linear guides

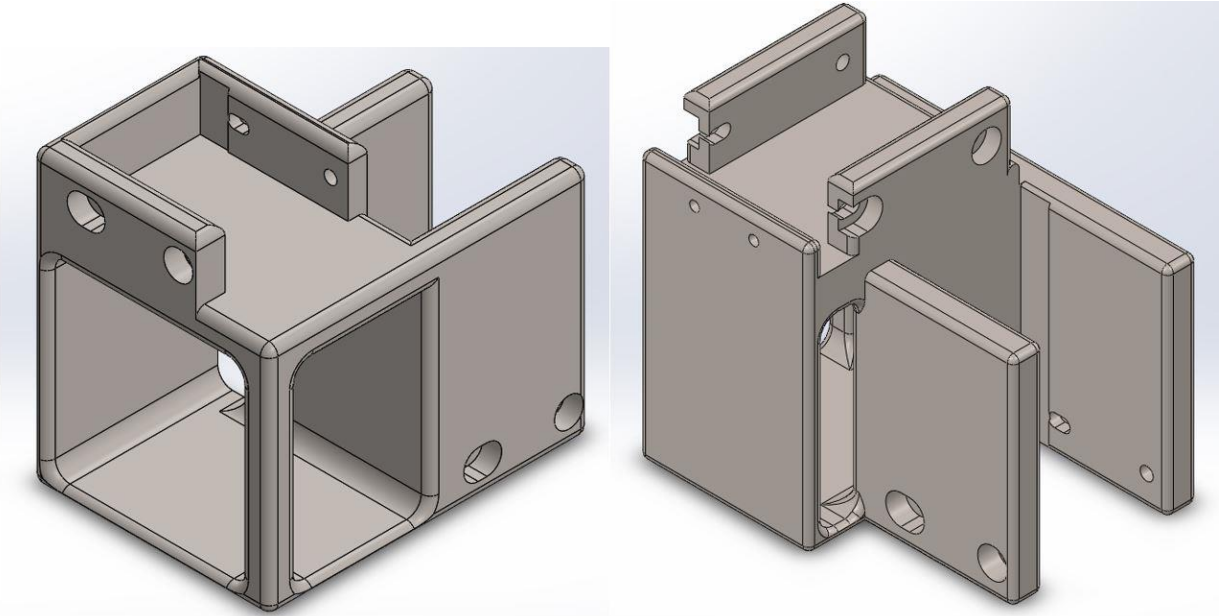


Figure 4. Corner blocks for positioning linear guides perpendicularly and for stable ground support

2. End-Effector Actuator and Housing

The end-effector actuator system is designed using the CAD software SolidWorks®. The actuator block consists of 12 components:

- 1 actuator housing
- 2 top compression springs (1" Long, 0.24" OD, 0.2" ID)
- 1 major compression spring (1" Long, 0.375" OD, 0.305" ID)
- 1 inner race
- 1 transducer cap
- 1 transducer
- 1 attachment bracket
- 1 motor clamp
- 1 stepper motor
- 1 driving cam

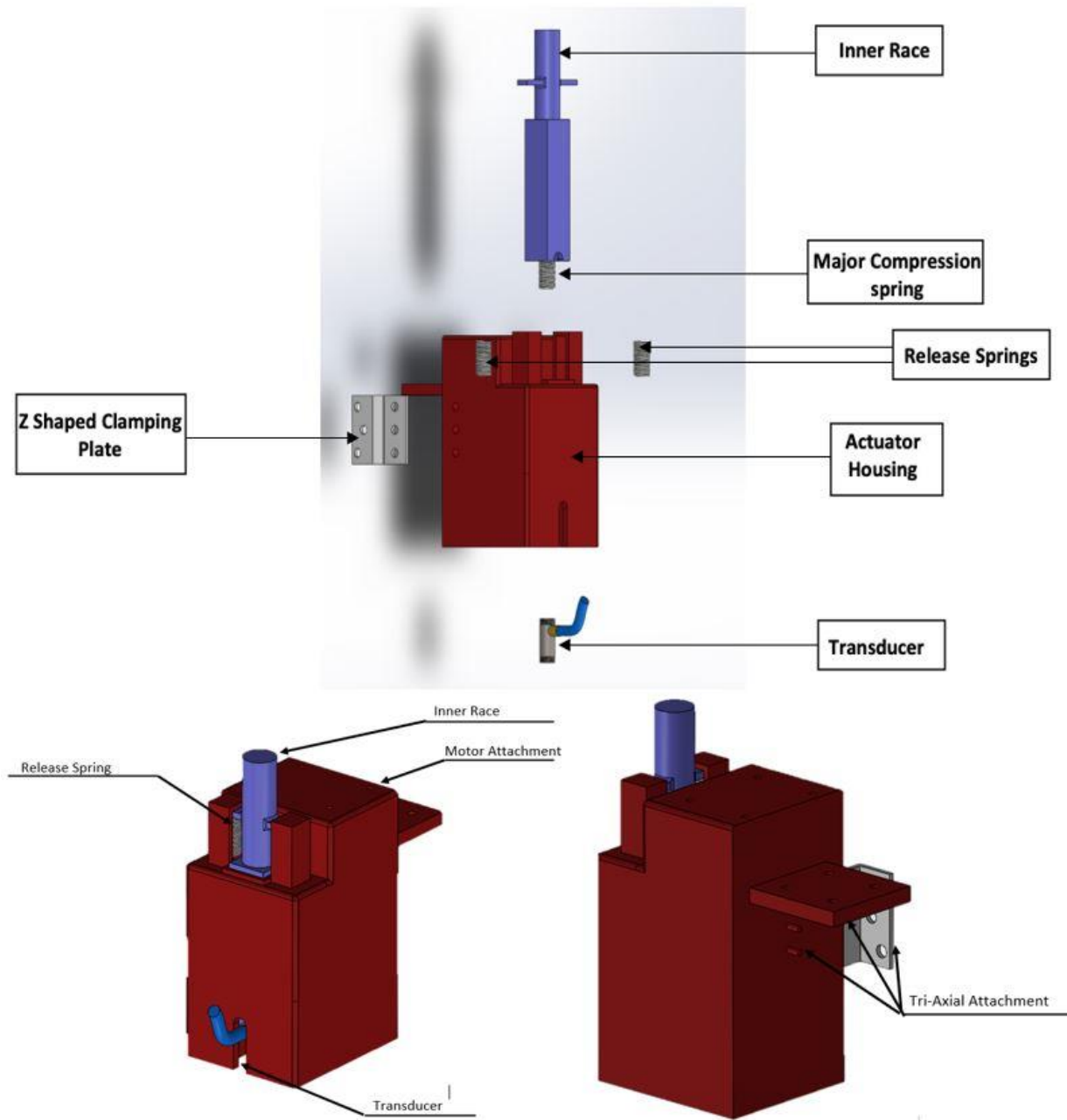


Figure 5. Exploded view and assembled view of end-effector actuator and housing

2.1. CAD Design

As shown in Figure 2, actuation is achieved using the cam that is rotated by the stepper motor to press upon the top of the inner race that is supported by two springs. The inner race houses

the transducer and as it descends the transducer is lowered toward the test specimen. The load on the transducer is controlled by the major compression spring connecting it to the inner race.

For the design of the end-effector actuator and housing, the following requirements need to be met:

- Tri-axial attachment of the actuator with the runner of the linear guides for better ground support to the transducer and minimized backlash error;
- Spring force equivalent to 500 grams of weight can be loaded onto the transducer;
- Transducer can travel at least 18 mm;
- Inner race must take on square shape for minimum quiver to minimize transducer placement error;
- Actuator housing can be 3-D printed with honeycomb in-fill to minimize its weight.

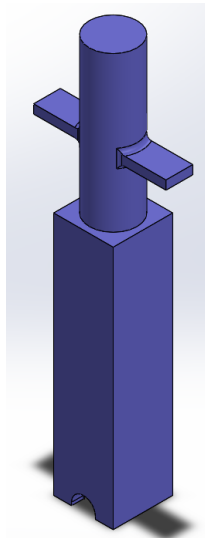


Figure 6. CAD design of inner race

The length and breadth of the block depend on the size of the motor used to actuate the cam mechanism. The size of the cam, height of the motor, and transducer travel distance decide the height of the towers that house the top compression springs.

In order to properly attach the housing, the attachments are designed in all three axes. For x-axis, we use the lock-key arrangement of two dowel projections, and for y and z-axis, we use the bolt and nut mechanisms. This tri-axial attachment shown in Figure 5 provides structural rigidity to the actuator housing as well as eliminates the possibility of micro-yielding to avoid backlash error when the transducer is in operation.

Within the actuator system, we have designed a square prismatic joint for the inner race that houses the transducer. The motivation behind the cross-sectional shape of a square is to minimize quiver and wobble. This design also eliminates undesirable self-rotation of the inner race and provides a guided course to the inner race for its motion. To accommodate the cable that is connected to the transducer, we cut a slot on the front face of the housing to allow for the free motion of the cable.

The inner race carries the transducer at one end via the major compression spring and bears the cam motion on the other end. The surface that is in contact with the cam is perfectly flat and smooth to minimize the friction. When the cam rotates it presses on the top surface and starts the downward motion of the inner race and the transducer. However, this motion is countered by the top compression springs that sit beneath the projections on the inner race. The function of the compression spring is only to pull the inner race back up after the cam begins its reverse journey. For the transducer end of the race, a circular atrium is made within which resides the major compression spring bonded to the bed of the atrium.

To attach the transducer to this spring, a special capping is devised. The capping is fabricated from a zinc nut that is grounded laterally to the dimension smaller than the atrium diameter and vertically to the height of 1.5 mm. This cap threads onto the transducer end. However, the cap still remains open on one side and the challenge arises when trying to attach the spring. A PLA material 3-D printed circular plate is made and reheated to the plastic point. Then, the cap is pressed onto it, bonding it permanently with the PLA plate. This plate is then attached to the spring via silicon rubber. Please note that the race has a small cut made on the atrium that allows for the transducer cable mount. It locks the transducer in place during experiment and hinders it from moving further inside the atrium. Lastly, a Z-shaped attachment plate is made to attach the housing to the linear guide stage. The following are the CAD drawings of the top housing assembly.

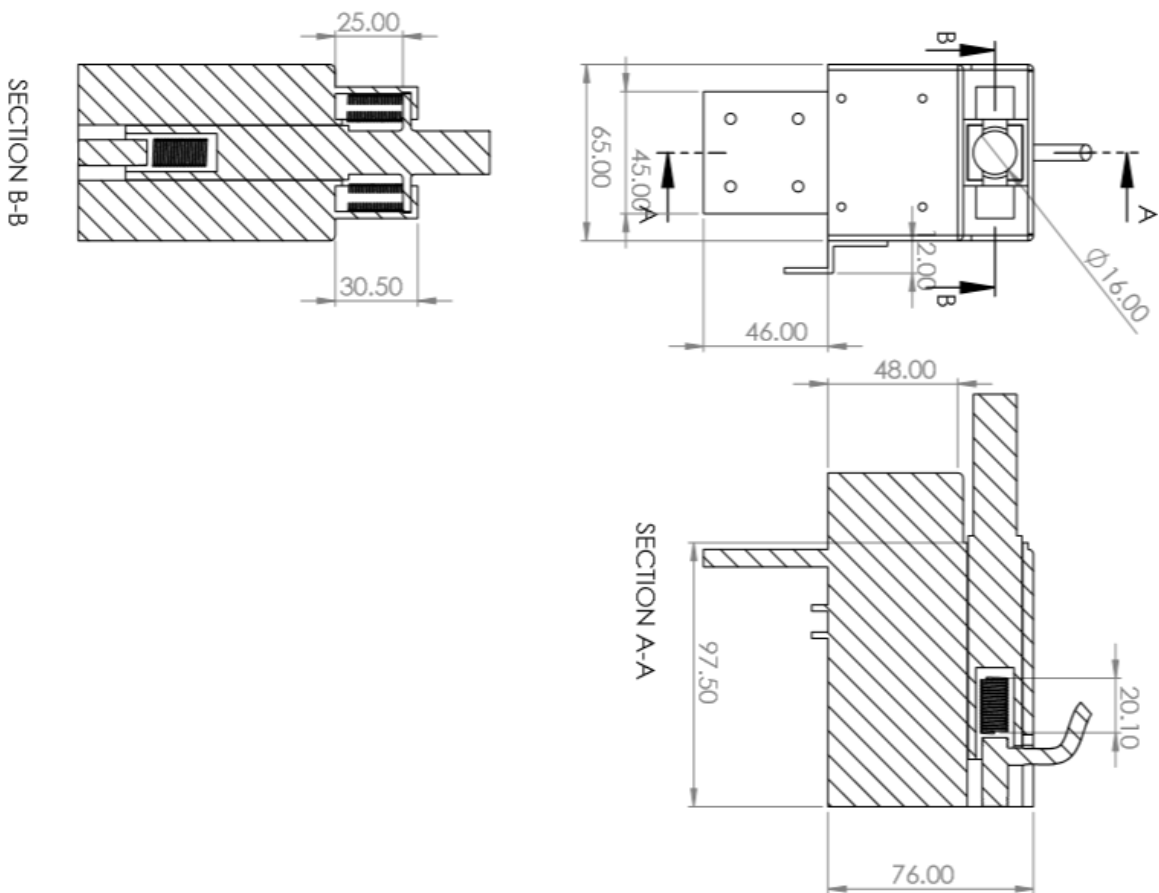


Figure 7. 2D sectional view of the end-effector actuator system

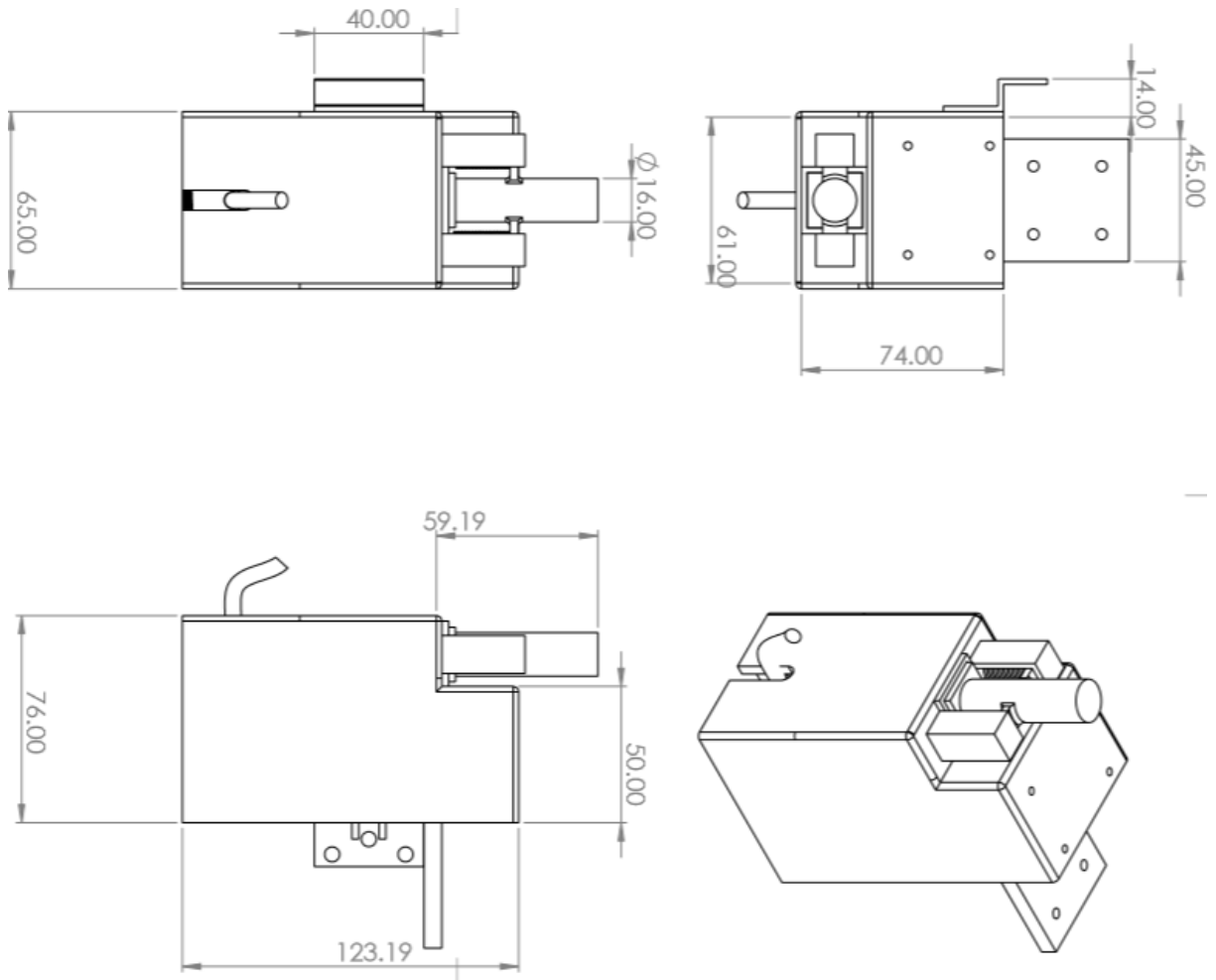


Figure 8. 2D sketch of the end-effector actuator system

Other than the system described above, we also designed a housing that allows the operation without the use of the top stepper motor. As shown in Figure 9, the top stepper motor mechanism is replaced by a weight slot that allows the user to put a weight on top. This is to accommodate the needs of the laboratory members whose experiments have fewer trials and less-rigorous accuracy requirements.

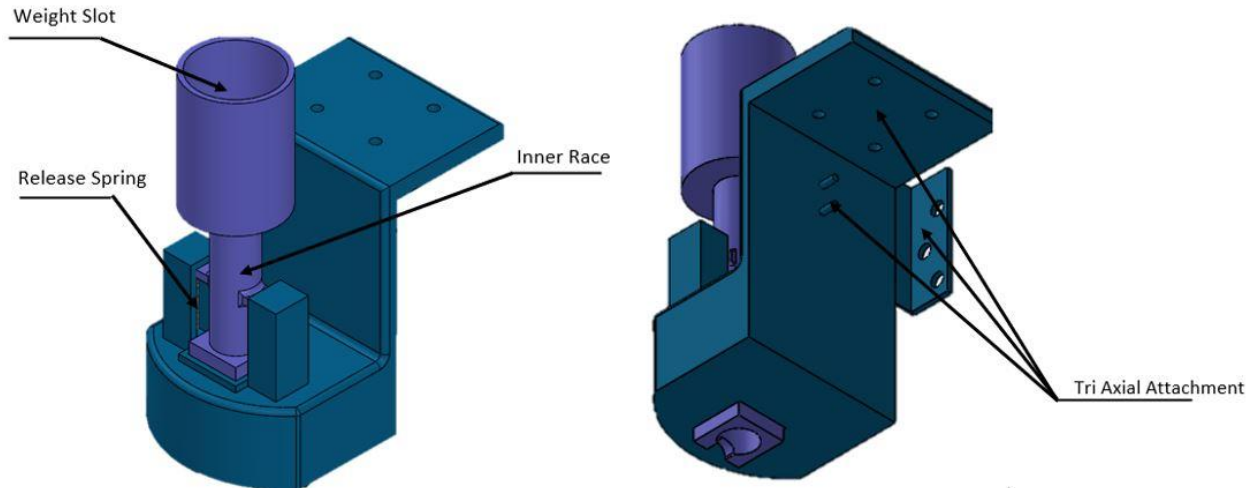


Figure 9. Modified end-effector system for manual operation

2.2. Finite-Element Analysis

In order to validate the design of the end-effector housing, the stress, strain and displacement states are simulated with the realistic loading conditions in the static structural test. Because the housing experiences multiple loads including the weight of the motor on top of the housing as well as the load that the motor exerts at the tower bases, the housing is only checked structurally.

The list of assumptions is listed as follows:

- Factor of safety is 0.3;
- Material complies with Hooke's law;
- Boundary Conditions do not vary during the load application;
- Von Mises theory is the criteria of failure.

The setup and specifications in SolidWorks® are listed as follows:

1. Test: Static Structural
2. Component Tested: Actuator Housing

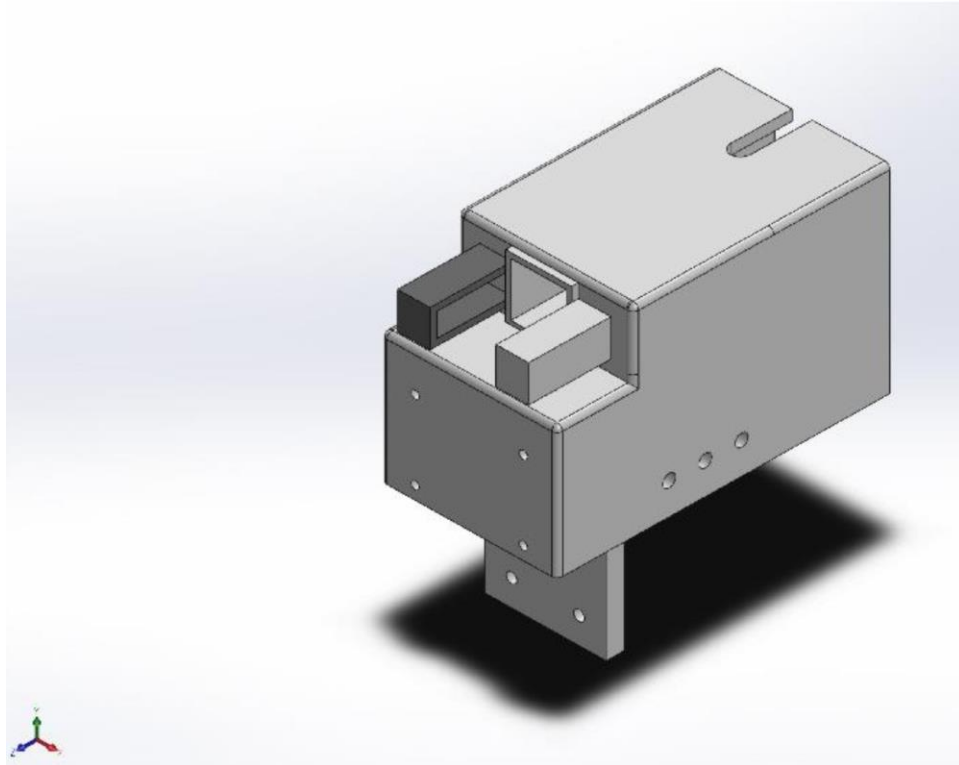


Figure 10. Actuator housing in the static structural test

3. Component Properties:

- Mass: 0.55 *kg*
- Volume: $5.38 \times 10^{-4} \text{ m}^3$
- Density: 1020 *kg/m*³
- Weight: 5.38 *N*

4. Material: ABS (Acrylonitrile butadiene styrene)

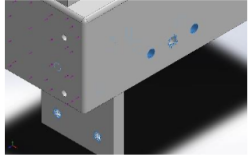
- Type: Linear Elastic Isotropic
- Tensile Strength: $3 \times 10^7 \text{ N/m}^2$
- Elastic Modulus: $2 \times 10^9 \text{ N/m}^2$
- Poisson's ratio: 0.394
- Mass Density: 1020 kg/m^3
- Shear Modulus: $3.189 \times 10^8 \text{ N/m}^2$

5. Units:

- Unit System: *SI (MKS)*
- Length/Displacement: *mm*
- Temperature: *Kelvin (K)*
- Angular velocity: *Rad/s*
- Pressure/Stress: *N/m^2*

6. Loading condition and Fixtures

- Fixed Constraint on fastening holes and dowel projections;
- Distributed force of 10-N on the top surface of the housing due to motor and clamp weight;
- Force (5-N) on the housing tower base where top compression springs are attached

Fixture name	Fixture Image	Fixture Details		
Fixed-1		Entities: 5 edge(s), 4 face(s) Type: Fixed Geometry		
Resultant Forces				
Components	X	Y	Z	Resultant
Reaction force(N)	1.76951e-06	-1.9297e-05	19.9999	19.9999
Reaction Moment(N.m)	0	0	0	0

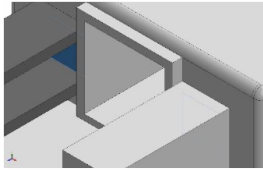
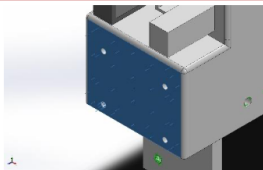
Load name	Load Image	Load Details
Force-1		Entities: 2 face(s) Type: Apply normal force Value: 5 N
Force-2		Entities: 1 face(s) Type: Apply normal force Value: 10 N

Figure 11. Summary of fixture features and loading conditions

7. Mesh

- Type: Solid Mesh
- Mesher Used: Blended Curvature-based mesh
- Jacobian Points: 4
- Maximum Element Size: 8.0 mm
- Minimum Element Size: 1.6 mm
- Quality: High
- Total Nodes: 47425
- Total elements: 30060

Model name: New Housing for Simulation
Study name: Static 1(-Default-)
Mesh type: Solid Mesh

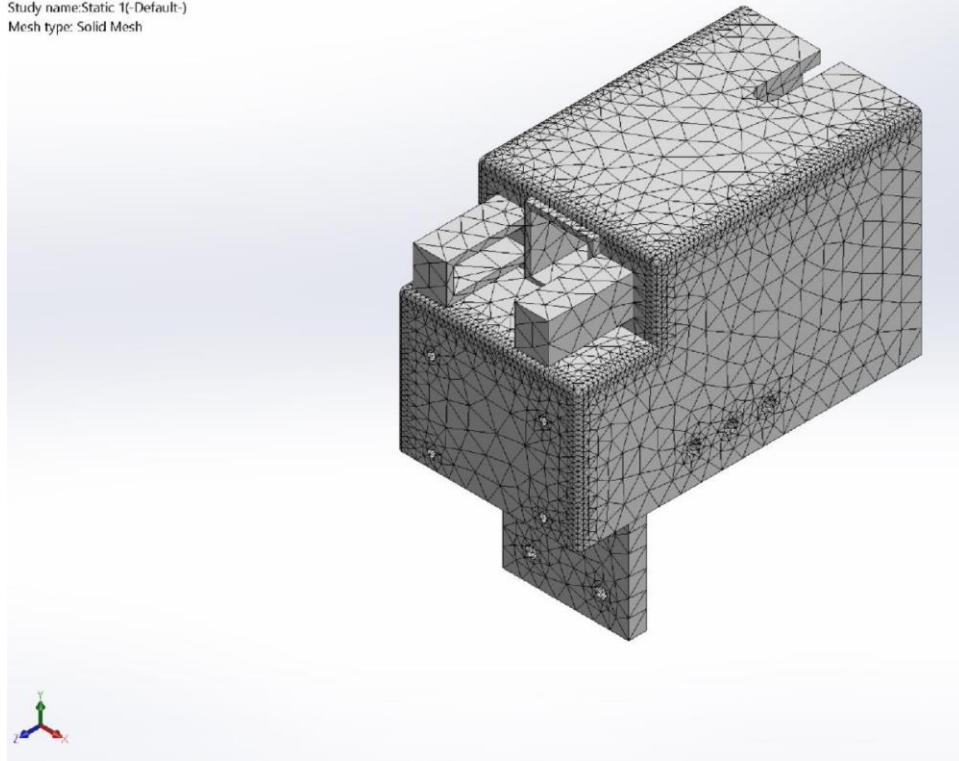


Figure 12. Illustration of the housing mesh condition

8. Results:

The results shown in Figure 13 validate that the maximum value of stress is within the safe limits and is about 100 times lesser than the tensile strength $3 \times 10^7 \text{ N/m}^2$.

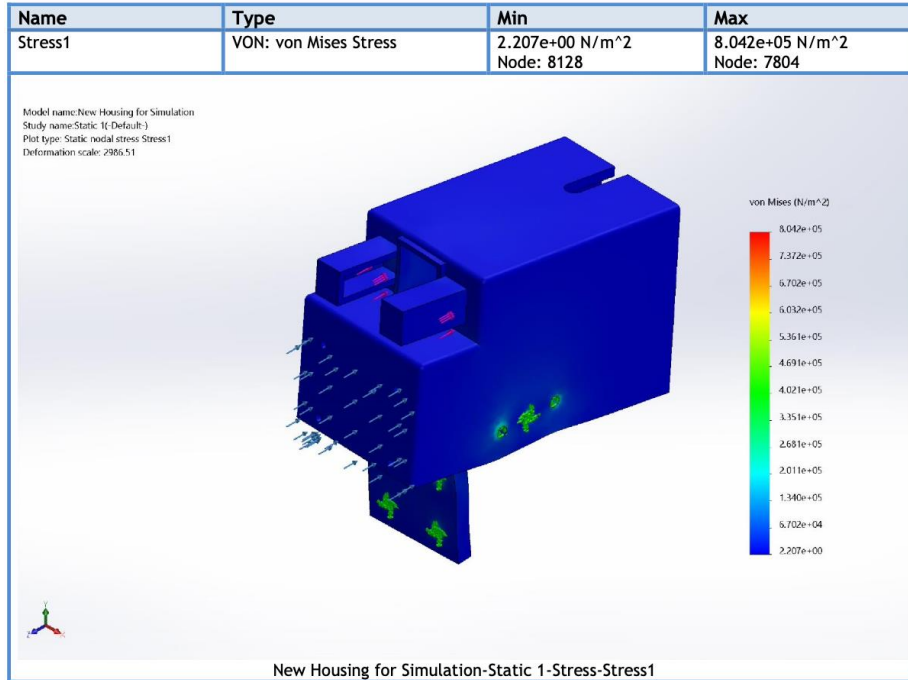


Figure 13. FEA result with the color gradient depicting stress value at different locations

Figure 14 validates that the maximum displacement is in the order of microns, which is safe when compared the scale of operation. The maximum strain value is validated as well.

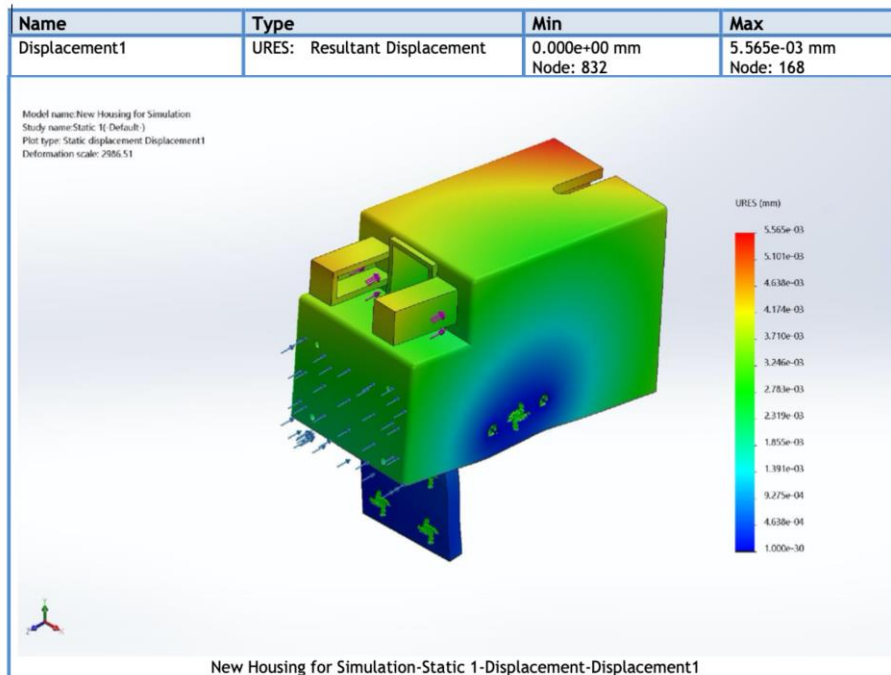


Figure 14. FEA result with the color gradient depicting displacement and strain value at different locations

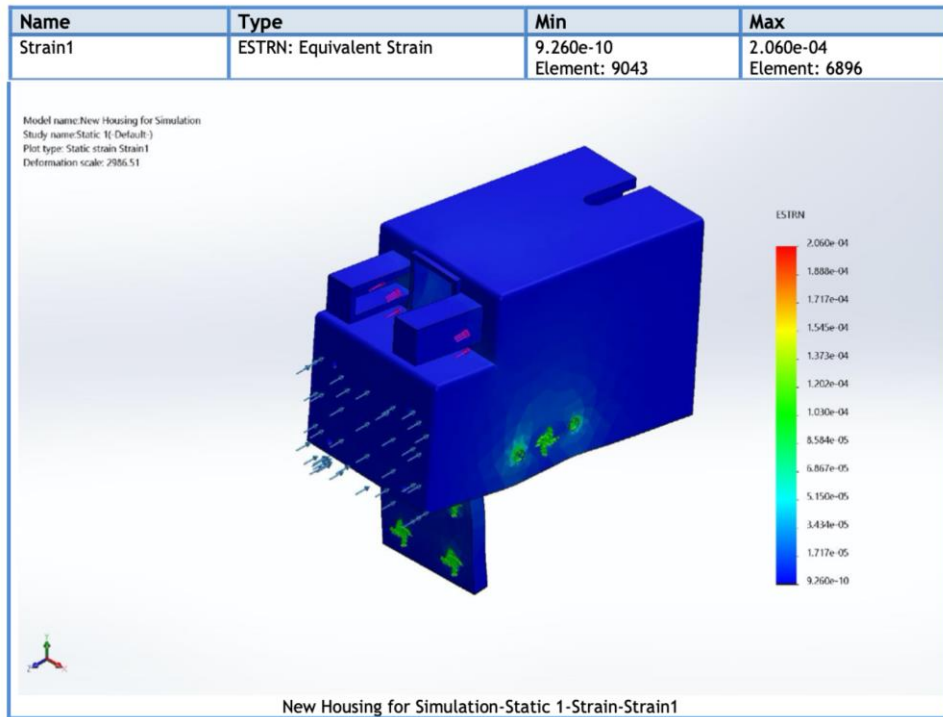


Figure 15. FEA result with the color gradient depicting displacement and strain value at different locations

9. Conclusion

The maximum stress, maximum displacement and strain are within the material property limits and the static structural test results for the actuator housing indicate safe operation for the given load conditions. Therefore, the design is validated and can be used for the end-effector operation.

2.3. Driving Motor Selection

Based on the experimental requirements provided by the laboratory members, the maximum transducer travel distance is 18 mm or 0.71". The two top compression springs placed on either side of the inner race extension needs to travel this distance. The selected spring was 1" in length and 0.24" in outer diameter with a spring rate of 2.7 lbs/in. Then, the required compression is:

$$F_{compression,1} = k\Delta x = 2.7 \times 0.71 = 1.92 \text{ lbs} = 8.54 \text{ N}$$

Since two of these springs are used, at maximum travel distance, the loading force that the top stepper motor needs to provide is:

$$F_{compression,2} = F_{compression,1} \times 2 = 8.54 \times 2 = 17.08 \text{ N}$$

Please note that this loading force requirement needs to take into account the size of the cam that connects the motor shaft and the top surface of the inner race. The design of the cam profile is elaborated in the following section.

The motor also needs to overcome the friction between the cam and the inner race in order to drive the mechanism. As the friction coefficient between PLA and PLA is estimated to be 0.492^[12], the total friction is given by,

$$f = \mu F_{compression,2} = 0.492 \times 17.08 = 8.403 \text{ N}$$

The maximum torque is applied when the farthest point of the cam profile is in contact with the inner race. For the cam profile used in our design, that point is 33-mm away from the center of the cam. Therefore, the necessary torque is given by:

$$\tau = fd = 8.403 \times 0.033 = 0.277 \text{ N} \cdot \text{m}$$

As a design requirement, a factor of safety of 4 is chosen for the motor. Therefore, the torque rating of the motor should be at least:

$$\tau_{motor} = 0.277 \times 4 = 1.1 \text{ N} \cdot \text{m}$$

Based on the calculations, a NEMA 23 bipolar stepper motor with 1.26 N-m holding torque, rated current of 2.8 A, and armature resistance of 0.9 Ω is chosen as the actuator.

2.4. Cam Profile Design

A radial cam mechanism is used for actuating the transducer^[9]. In order to determine the optimal cam profile, the following requirements are set:

- Travel distance of the transducer needs to be 18 mm;
- Base circle radius needs to be 15 mm to account for the size of the motor;
- Cam needs to have dwell at minimum radius;
- Cam profile needs to be symmetric.

To ensure smooth actuation, a constant velocity curve was chosen for the cam profile. This results in an Archimedes spiral^[11]. In parametric form, the following spiral equations are calculated:

$$x_t = \left(\frac{119}{3} - \frac{40\theta}{3\pi} \right) \cdot \cos\theta$$

$$y_t = \left(\frac{119}{3} - \frac{40\theta}{3\pi} \right) \cdot \sin\theta$$

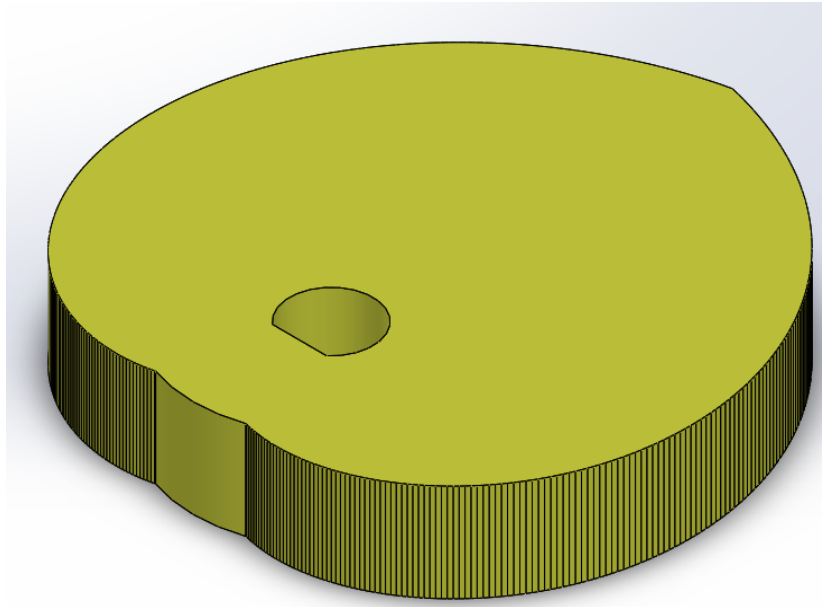


Figure 16. Illustration of the cam profile

In this study, θ varies from $\frac{\pi}{6}$ to $\frac{\pi}{2}$ to create one side of the symmetric cam. The shock due to high acceleration ^[9] from the cam profile is absorbed by the compliant spring system in the mechanism. The cam profile is shown in Figure 15.

2.5. Assembly of System

When the linear guide system is assembled as shown in Figure 3, the end-effector actuator systems are integrated into the system. The final assembly of the Automated Grid System is shown in Figure 16. A demonstration of the final product is included in the later part of this thesis.

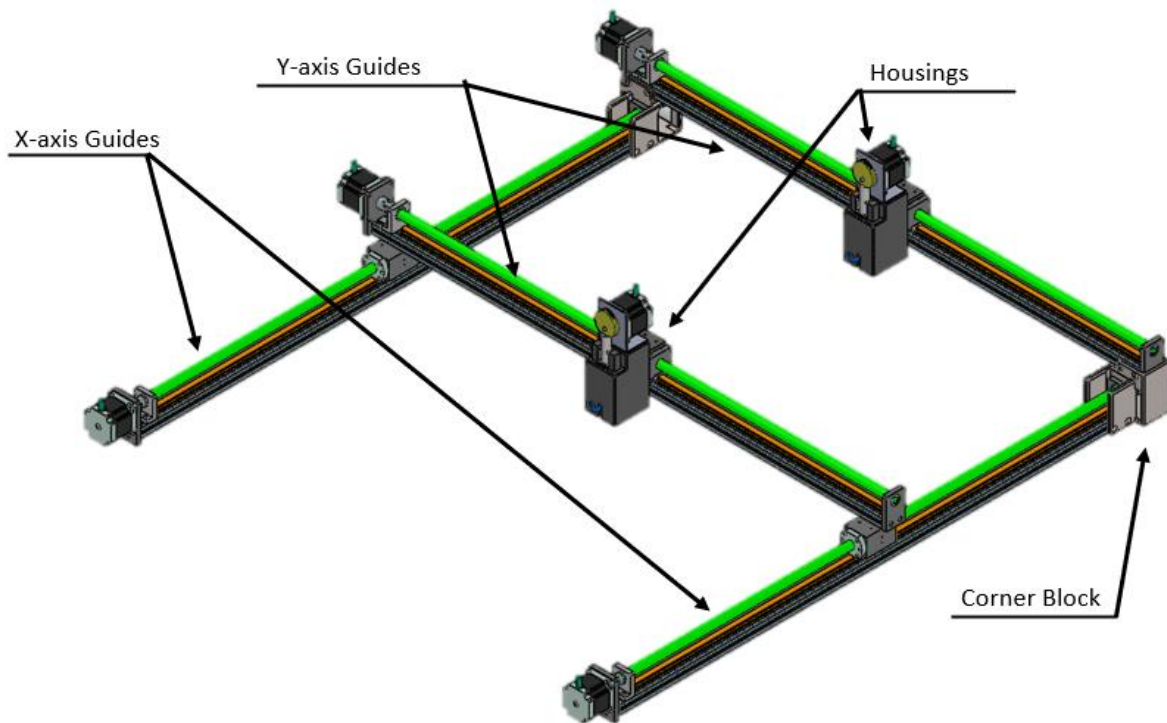


Figure 17. Assembly of the Automated Grid System

2.6. Workspace of System

The highlighted box in yellow represents the reachable workspace of the Automated Grid System as shown in Figure 17. The end effector has range of motion of 900-mm in the x-axis, 930-mm in the y-axis, and 18-mm in the z-axis. Therefore, the dimensions of the reachable workspace in x, y, z axes respectively are 900 x 930 x 18 mm.

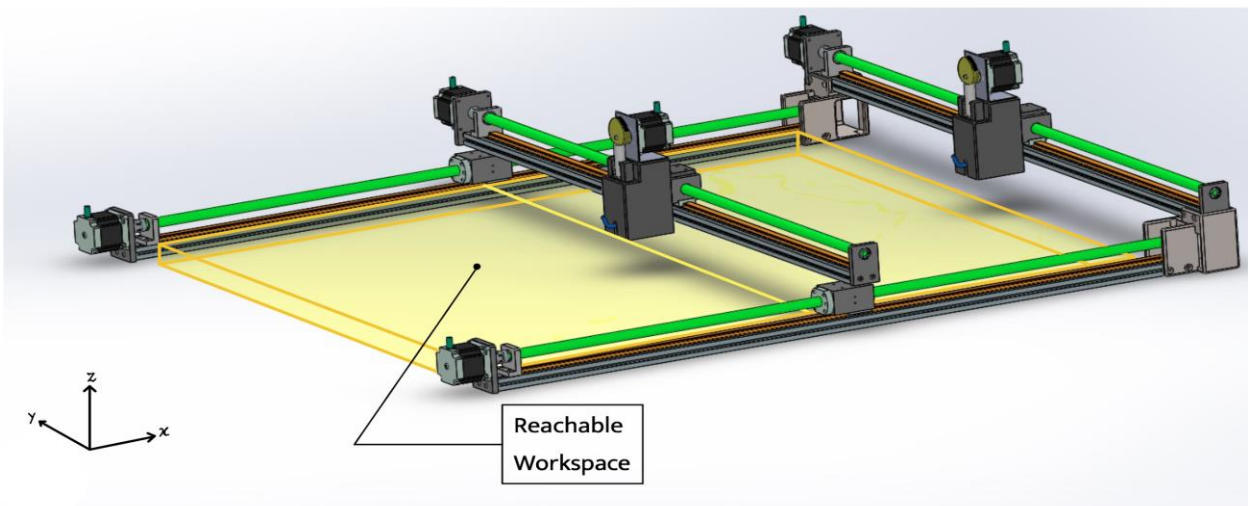


Figure 18. Reachable workspace of the Automated Grid System (900 x 930 x 18 mm)

III. Electrical Design

1. Linear Guides

The linear guide system has five groups of electrical components: one DC power unit, one AMC4030 controller, three FMDD50D40NOM drivers, two limit switches, and two button switches. The wiring diagram is shown in Figure 16.

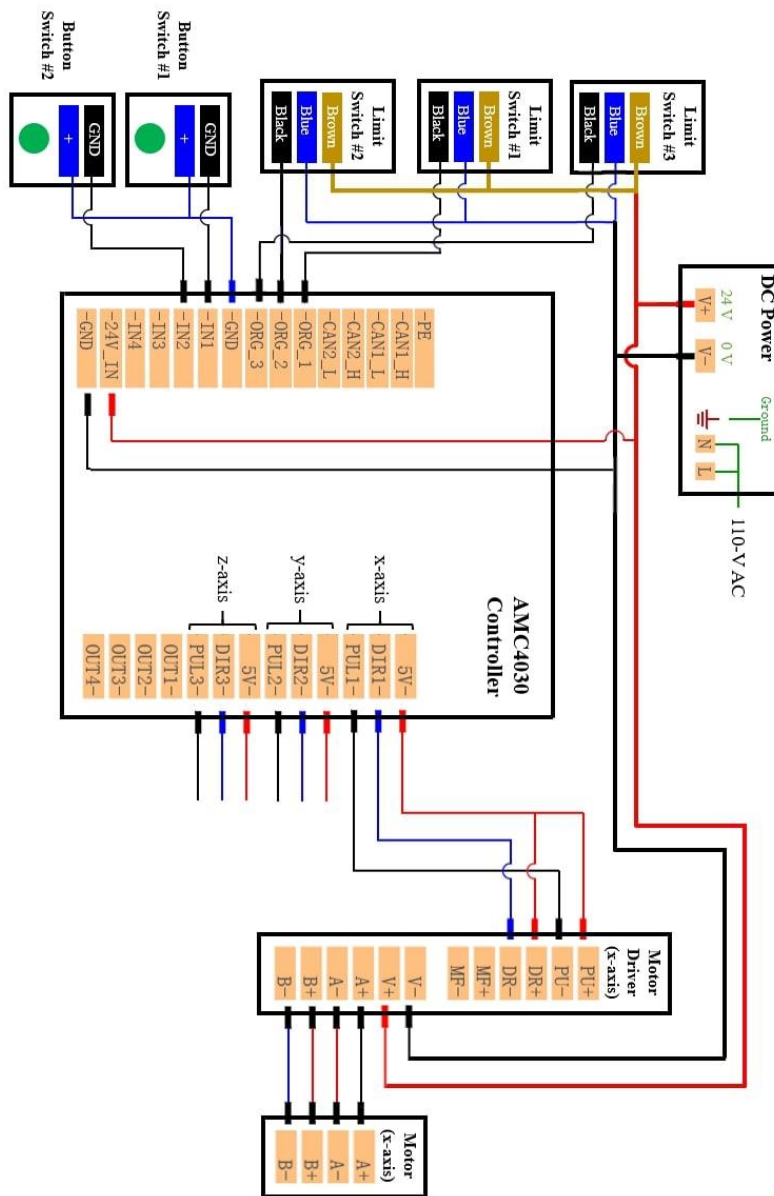


Figure 19. Wiring diagram of the linear guide system

The DC power unit takes the standard 110 V AC voltage input. The output high level (24 V) and low level (0 V) are used by the entire system. A power cable is designed and fabricated for the connection to the power outlet. For the safety of operation, please do not change or modify this cable.

The AMC4030 controller is connected to the motor driver of each axis. The motor driver is then connected to the stepper motor situated at the top of the linear guide. Please note that in the wiring diagram, the wiring is omitted for the y- and z-axis for better demonstration. The connections for these axes are identical to that of the x-axis.

The limit switches are in place for the homing calibration procedure. For each axis, when the stage is within 2-mm of the limit switch, the system sets the current position of the stage as zero and calibrates that axis. The button switches are in place as input sources for the software. This application will be discussed in the later section. In addition, an emergency stop button (not shown in the wiring diagram) is embedded in the system to stop all movements when pressed.

2. Top Stepper Motor

The stepper motor chosen for the end-effector actuator system is the NEMA 23 bipolar stepper motor. It is driven by the DM542 stepper motor driver and controlled by the Arduino Uno controller that generates the direction and rotation limit logic. Because the driver is capable of micro-stepping, high angular accuracy can be achieved when actuating the cam. The wiring diagram is shown in Figure 17.

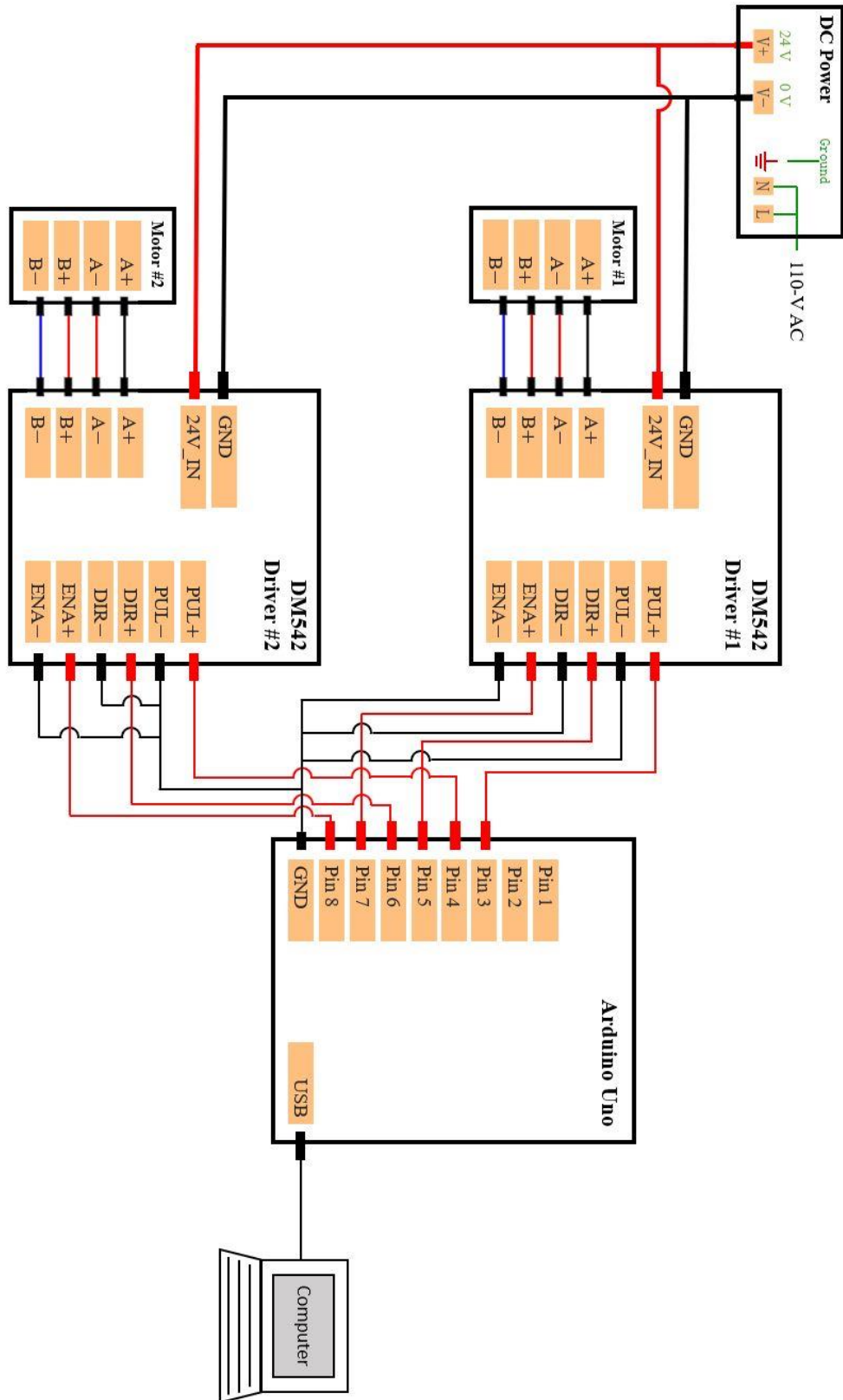


Figure 20. Wiring diagram of the end-effector actuator system

With an operating voltage of 24 V, the current through the motor armature would be 26 A without proper drive pulsing. Therefore, a dedicated high-current stepper motor driver, such as the DM542, is necessary for this setup. For the initial test, 1600 steps/revolution was set for the motor drive with equal rotation in clockwise and counterclockwise directions.

The Arduino sets the STP, DIR and ENBL pins on the driver to program the number of steps per revolution, direction of revolution, and to enable the driver respectively. Through the Serial connection with the computer, the user can enter the rotation of the cam as the number of steps to be rotated, thus setting the position of the transducer in the z-direction. The software reads the input and sends corresponding number of pulses to the driver. For each pulse from the Arduino, the driver generates a high-current pulse required to actuate the stepper motor. After reaching the required angular position, the enable pin is reset and the driver is disabled until the next input is received.

Two such systems are used to actuate the excitation transducer and the receiving transducer, respectively. The Arduino is connected to both DM542 drivers, but it is able to control each motor individually. Angular position input is provided through Serial input for both.

IV. Software Design

In order to simplify the operation of the automated grid system, a graphical user interface (GUI) is designed in collaboration with Fuyu Technology Inc. This GUI is modified based on a previous operation software to accommodate needs specific to the Material Degradation Laboratory. The software layout, as shown in Figure 18, consists of three primary sections: 1) language selection, 2) operation tabs, and 3) operation window. Currently, English and Mandarin Chinese are available to the user as the interface language, but it is made available to add new languages easily. In the operation tabs section, there are five tabs: “Connect Controller (CNCT CTL)”, “Manual Operation (MNL OPER)”, “Set Parameters (Set PARM)”, “Edit Program (Edite PGM)”, and “About”. When a tab is selected, it is highlighted in green, and the corresponding operation window opens on the right. These tabs and the respective operation windows will be discussed in detail in the following section.

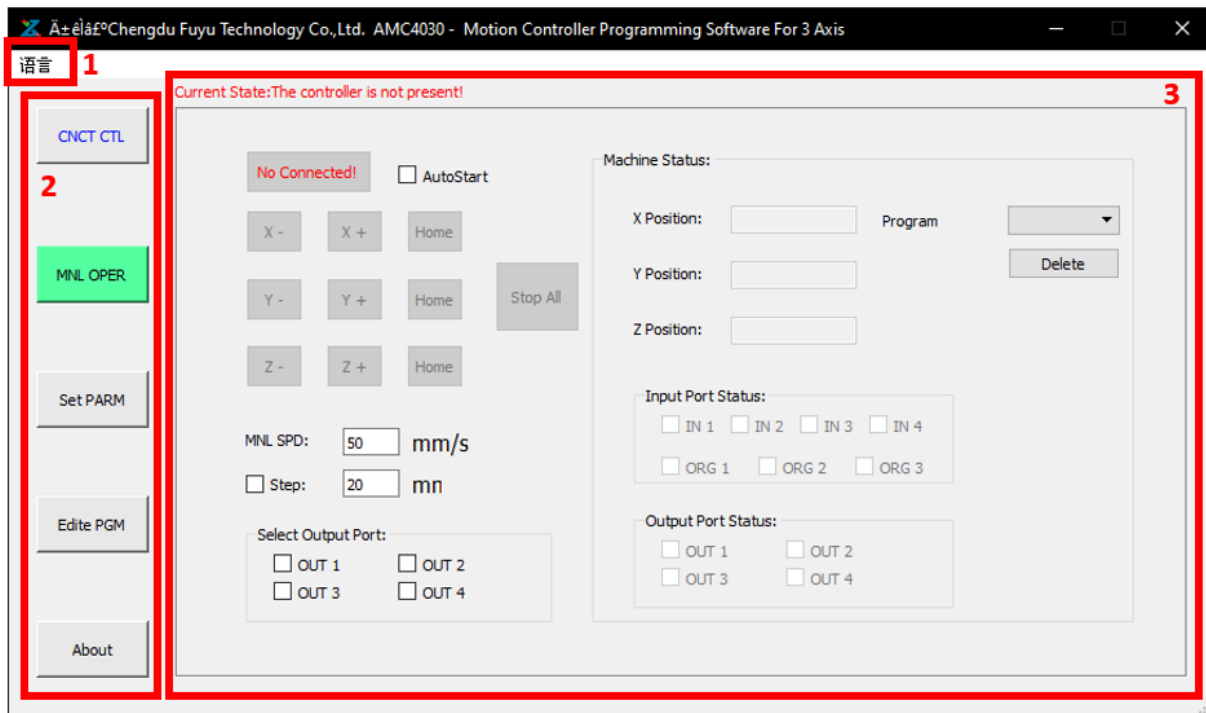


Figure 21. Software layout: 1) language selection, 2) operation tabs, and 3) operation window

1. Connect Controller (CNCT CTL)

When the controller is plugged into the computer, it will be detected by the software and marked available to connect through wire communication. When the user presses the “CNCT CTL” tab, the software establishes the communication protocol and shows if the connection is successful. Once the state is switched to “Connected”, all the options in the other tabs are available to the user.

2. Manual Operation (MNL OPER)

The automated grid system allows the user to manually operate the system and move the transducer to the desired location. In the Manual Operation tab, there are 1) the manual control panel and 2) the machine status panel.

The manual control panel consists of the “AutoStart” button, the movement control of each axis, the speed control (MNL SPD), the “Step” button, and the output voltage logic level buttons (OUT1 to OUT 4). When the “AutoStart” button is ticked, when the program is loaded, it enters the manual operation mode instead of running the preset program in the “Edite PGM” tab. Below the “AutoStart” button, in the movement control of each axis, the user can specify the direction of the stage movement in the positive and negative direction. The positive direction is away from the motor. When the “Home” button is pressed, the stage moves in the specified homing direction till the calibration sensor detects it and stops the movement. The homing direction can be selected in the “Set PARM” tab. The speed control (MNL SPD) allows for the tuning of stage movement speed with the maximum at 250-mm/s. When the “Step” button is ticked, one press of the positive

of negative manual movement button (e.g. X - or X +) indicates that the stage will move in the corresponding direction for the specified distance (20-mm in the shown settings).

The output voltage logic level buttons take advantage of the fact that the AMC4030 controller outputs high-level voltage signal by default. When the output button is ticked, the output voltage becomes low-level. Therefore, there is a voltage difference between the corresponding IN port and the open OUT port, which can be used for different applications. For example, the four different output ports can be connected to four LEDs in different colors to keep track of the experiment trials. To achieve this, for one of the LEDs, the positive should be connected to the IN 1 port of the controller while the negative to the OUT 2 port. Please note that in order to prevent any complications, do not use button switches in series with the LEDs or any other electronic devices between the same pair of IN-OUT ports.

The machine status panel displays the current position of the stage on the top. During the calibration process at the beginning of experiments, each position reading will be zeroed when the calibration sensor detects the stage. On the bottom, the software shows if the IN, ORG, and OUT ports are in use. Please note that this function can be used to debug the circuits introduced by the user (e.g. the LED circuit mentioned in the previous paragraph).

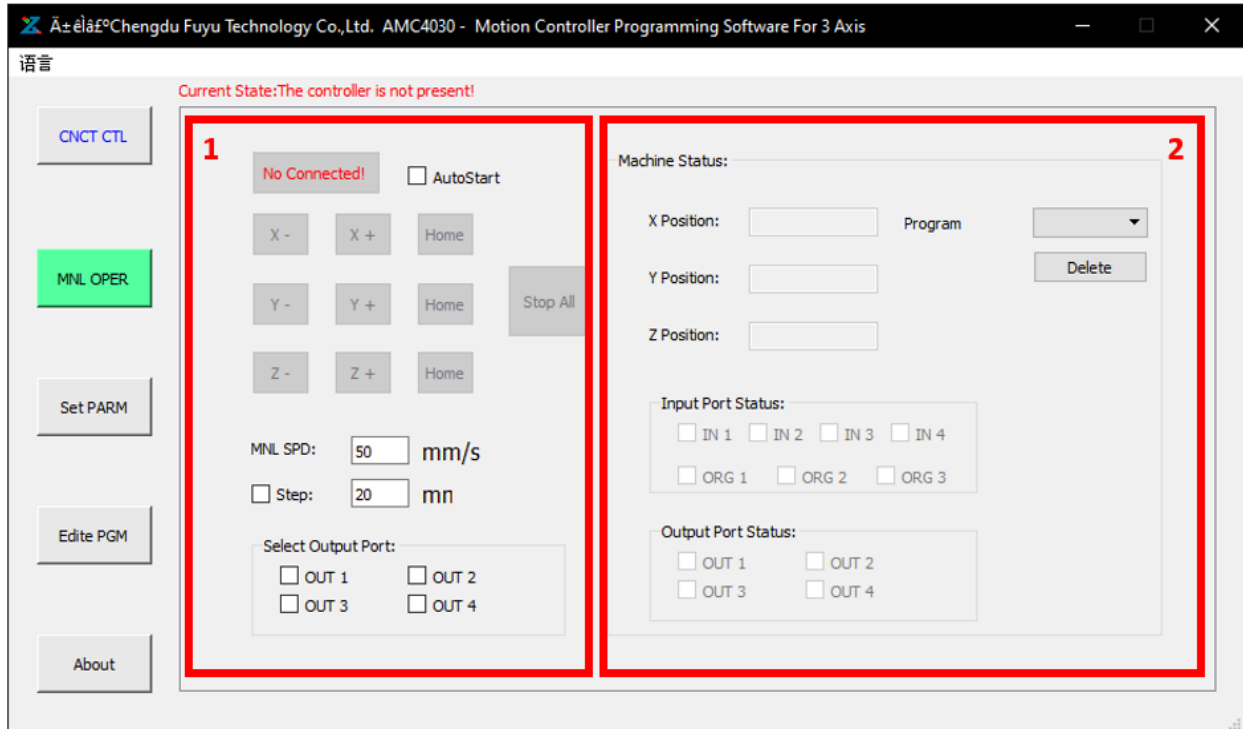


Figure 22. Manual Operation tab interface: 1) manual control panel and 2) machine status panel

3. Set Parameters (Set PARM)

Before any operations are initiated, the parameters of the automated grid need to be input and verified. In total, six parameters are required by the software for each axis: DIST, Pulse NUM, Max DIST, Home DIR, Home SPD, and ORGN OFST.

The “DIST” parameter represents the distance that the stage moves in millimeter when one rotation of the motor is completed. This value is 10-mm for the NEMA 23 2-phase motor (56-mm length) used in the ball-screw linear motion guides. The “Pulse NUM” parameter is the number of pulses the driver needs to send to the motor to complete one full rotation. This value is dependent on the driver model. For the AMC4030 controller, this value is 5000. Please note that any value lower than 5000 can also be used to override the driver input in certain cases. When the value is

lower, the motor rotational speed is reduced, therefore lowering the movement speed of the linear guide. The “Max DIST” parameter is the maximum distance the stage can travel on the linear guide. For the FSL40 linear guide, this number is 1000-mm. The “Home DIR” parameter is the direction in which the stage returns to zero. This parameter is useful during the calibration process. Typically, the N-direction is when the stage moves toward the motor. The “Home SPD” parameter specifies the speed at which the stage returns to the home or zero position. Please note that the maximum speed is 250-mm/s. The “ORGN OFST” parameter is the maximum distance the motor will try to move the stage after the stage touches the stopper. This offset is created as a buffer region to avoid damaging the device. This number is 5-mm by default. Please note that the user cannot modify the other parameters, such as the system acceleration (SYS ACC). This is in place to protect the electrical system.

The user can also load previously saved parameter settings via “Loade PARM”, save the current parameter settings via “Save PARM”, or restore the default settings via “RSTR SET”. Please note that the default settings may not be optimal for the individual experiment requirements.

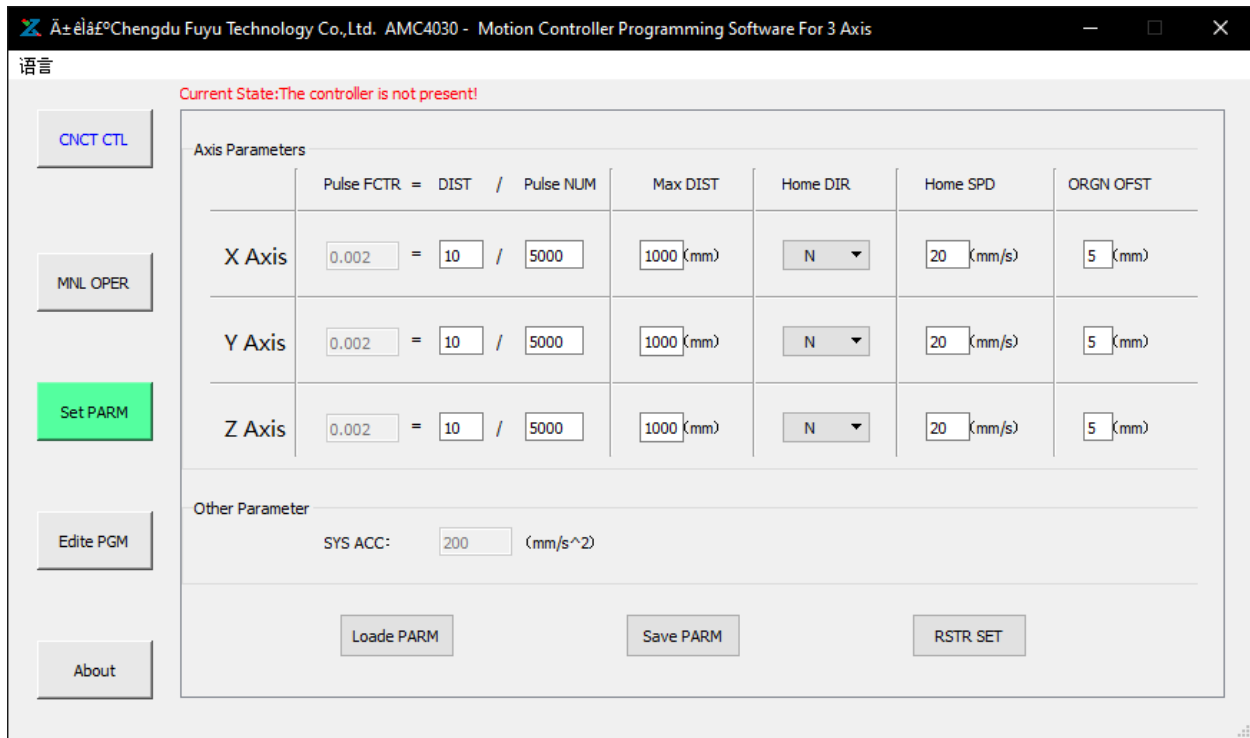


Figure 23. Set Parameters tab interface

4. Edit Program (Edite PGM)

Besides the manual mode, the software also allows the user to operate the system with a preset program. Figure 21 shows the interface of the “Edit Program” tab. The main window shows the current program and its commands. The user can select actions on the right to add, delete, and modify the current program. In addition, the software allows the user to save the current program or load a preset program.

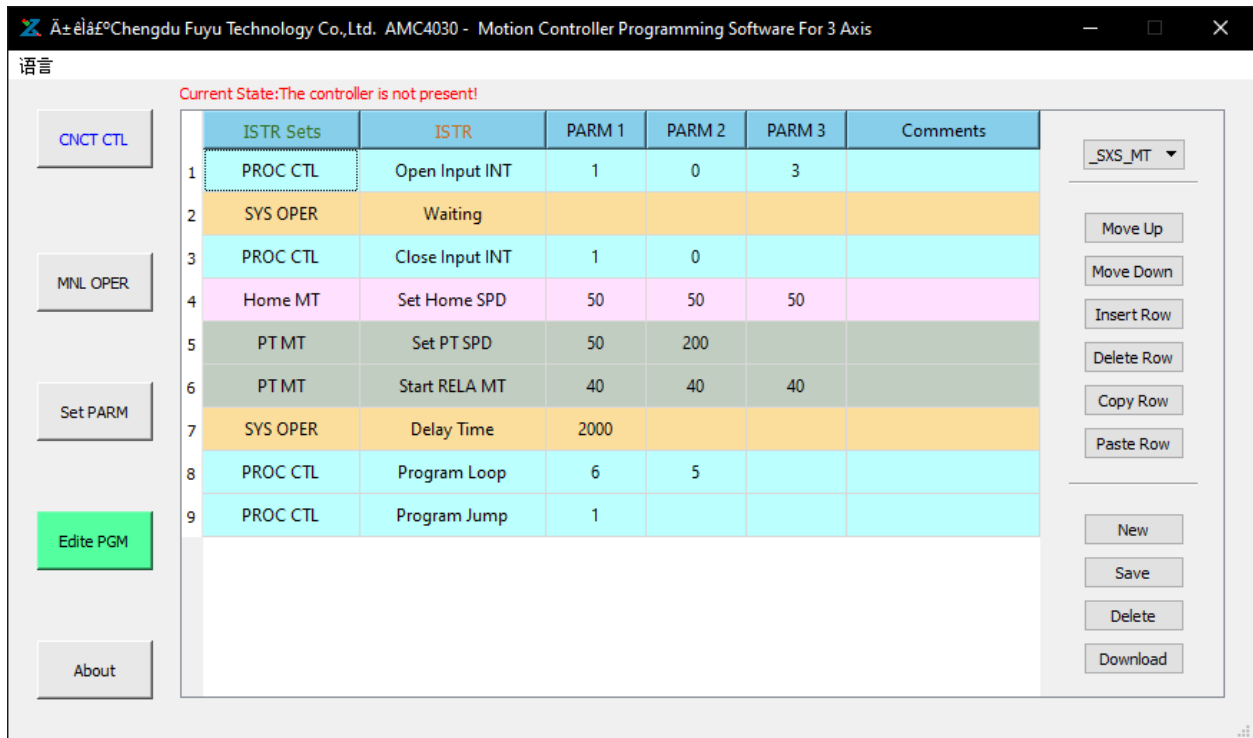


Figure 24. Edite Programs tab interface

The program can consist of multiple commands selected from a list of 13 commands. These available commands are listed in Figure 21 with the respective detailed description.

ISTR Set	ISTR	PARAM 1	PARAM 1 Notes	PARAM 2	PARAM 2 Notes	PARAM 3	PARAM 3 Notes	ISTR Notes
SYS OPER	Stop All	x	x	x	x	x	x	System is turned off and the data are cleared. No further commands can be executed unless the program is restarted.
	Delay Time	Positive integer	[ms]	x	x	x	x	System stands by till the preset wait time in PARAM 1 is reached. Maximum wait time is 20 days. System is stopped. Only "Open Input INT" command can be executed.
	Waiting	x	x	x	x	x	x	Jump to the target line of command and execute.
PROC CTL	Program Jump	Positive integer	Index of target line	x	x	x	x	When program reaches "Program Loop" line of command, program jumps to the previous line of command specified by PARAM 1, executes all commands in between till the "Program Loop" is reached again. The number of loops is subtracted by 1 each time.
	Program Loop	Positive integer	Index of target line	Positive integer	Number of loops	x	x	When a high- or low-level signal (specified by PARAM 2) is detected at the input port specified by PARAM 1, the program jumps to line of command specified by PARAM 3.
	Input Jump	1/2/3/4		0/1	0 for low level, 1 for high level	Positive integer	Index of target line	The system continuously monitors if the event (specified by PARAM 2) happens. When the event happens at the input port specified by PARAM 1, the program jumps to line of command specified by PARAM 3.
Output OPER	Open Input INT	1/2/3/4	Index of input ports: IN1/IN2/IN3/IN4	0/1	0 for high to low, 1 for low to high	Positive integer	Index of target line	The system continuously monitors if the event (specified by PARAM 2) happens. When the event happens at the input port specified by PARAM 1, the program stops any continuous monitoring.
	Close Input INT	1/2/3/4		0/1		x	x	Set voltage of the output port (specified by PARAM 1) to desired level (specified by PARAM 2).
	Set Output	1/2/3/4	Index of input ports: OUT1/OUT2/OUT3/OUT4	0/1	0 for low level, 1 for high level	x	x	Set the homing speed of all three axes in [mm/s]. Acceleration is "SYS.ACC" in "Set PARAM" tab.
Home MT	Set Home SPD	Positive number	Homing speed for x-axis in [mm/s], maximum value 250	Positive number	Homing speed for y-axis in [mm/s], maximum value 250	Positive number	Homing speed for z-axis in [mm/s], maximum value 250	Set the movement speed and acceleration for all axes. Keep PARAM 2 at 200 for most cases.
	Set PT SPD	Positive number	Movement speed for all axes in [mm/s], maximum value 250	Positive number	Acceleration for all axes in [mm/s], recommended value 200	x	x	Set displacement values in each axis. Displacement can be positive or negative. The positive direction is away from the stepper motor.
	Start RELA.MT	Number	Displacement in x-direction in [mm]	Number	Displacement in y-direction in [mm]	Number	Displacement in z-direction in [mm]	Set the desired end location. This command must follow a homing process with "Start RELA.MT".
PT MT	All Axis MT	Positive number	x-coordinate in [mm], maximum value 1000	Positive number	y-coordinate in [mm], maximum value 1000	Positive number	z-coordinate in [mm], maximum value 1000	

Figure 25. List of available commands to preset the program

It is worth noting that the commands “Input Jump”, “Open Input INT”, and “Close Input INT” require a voltage logic level input into the controller. For instance, the input port IN1 can be connected to a switch button that switches between low-level (0-V) and high-level (24-V). If the program has the command line “Open Input INT” with PARM 1 = 1, PARM 2 = 1, and PARM 3 = 3, it means when the voltage level switches from low-level to high-level at input port IN1, the program will jump to command line 3 and execute. Most switch buttons are at low-level when the button is un-pressed by default. Therefore, when a switch button connected to IN1 is pressed, the voltage level switches from low to high, satisfying the condition in PARM 2. The program will then jump to command line 3 and execute. This logic applies to the other two commands listed above as well.

A sample program that has been tested is shown and explained below to further help the user understand the software.

Example: Incremental movement of transducer

1. The system waits for the input signal from a switch connected to IN1. When the switch changes the voltage level from high to low, the program jumps to command line 2;
2. The system performs the homing calibration with homing speed 50 mm/s for all axes;
3. The system sets the movement speed at 50 mm/s and acceleration at 200 mm/s for all axes;
4. The system moves the transducer for 40 mm in the positive direction for all axes;
5. The system waits for 2000 ms, or 2 seconds;

6. The system jumps back to command line 4 and moves the transducer again. The process is looped for 5 times;
7. The system jumps back to command line 1 and waits for the input signal from the switch.

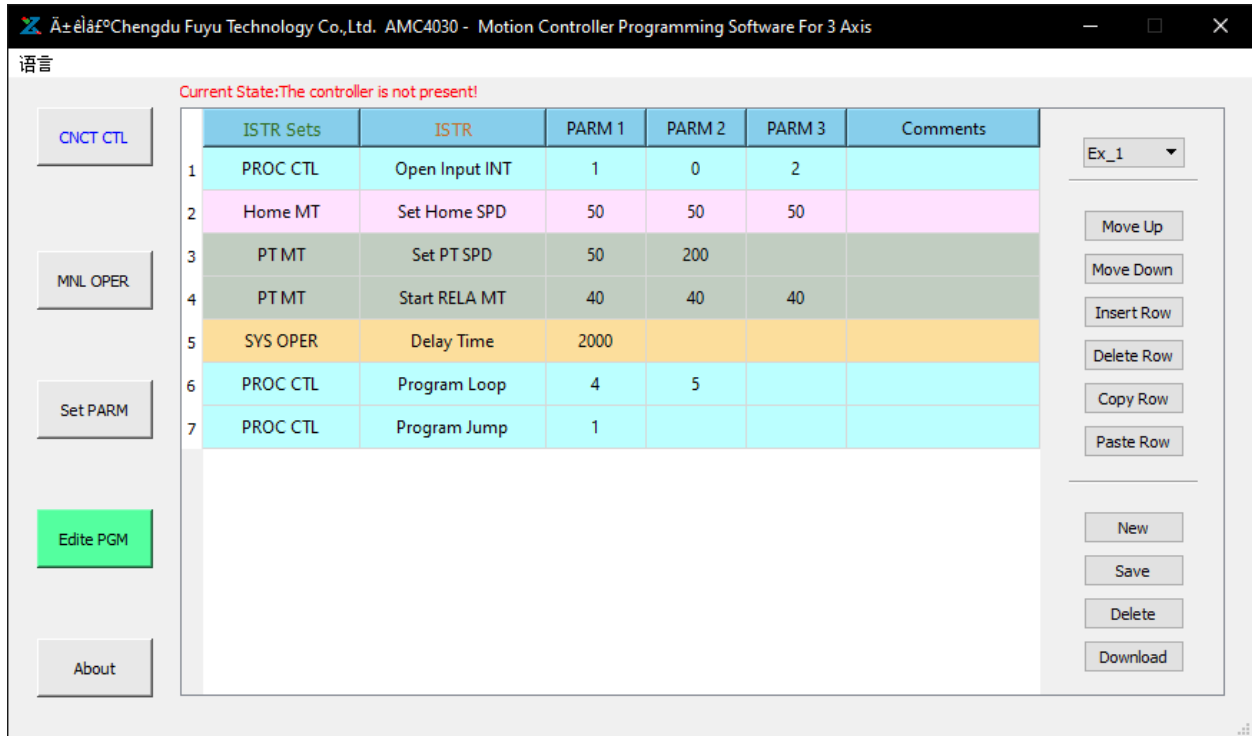


Figure 26. Example program: incremental movement of transducer

5. Company and Laboratory Information (About)

The “About” tab includes information about Fuyu Inc. as well as the Material Degradation Laboratory supervised by Prof. Ajit Mal. However, if the user encounters any technical difficulties, it is highly encouraged to contact Yichi Zhang at yichizhang@engineering.ucla.edu before attempting any fixes.

V. Product Demonstration

This section demonstrates the final product that was built following the design guidelines. Figure 27 shows the end-effector actuator system attached to the linear guide stage. Figure 28 and 29 demonstrate the final assembly that is currently in the laboratory. Figure 30 and 31 show the wiring of the linear guide system and the end-effector actuator system, respectively. Please note that the current wire management is not optimal and its improvement is part of the future work.

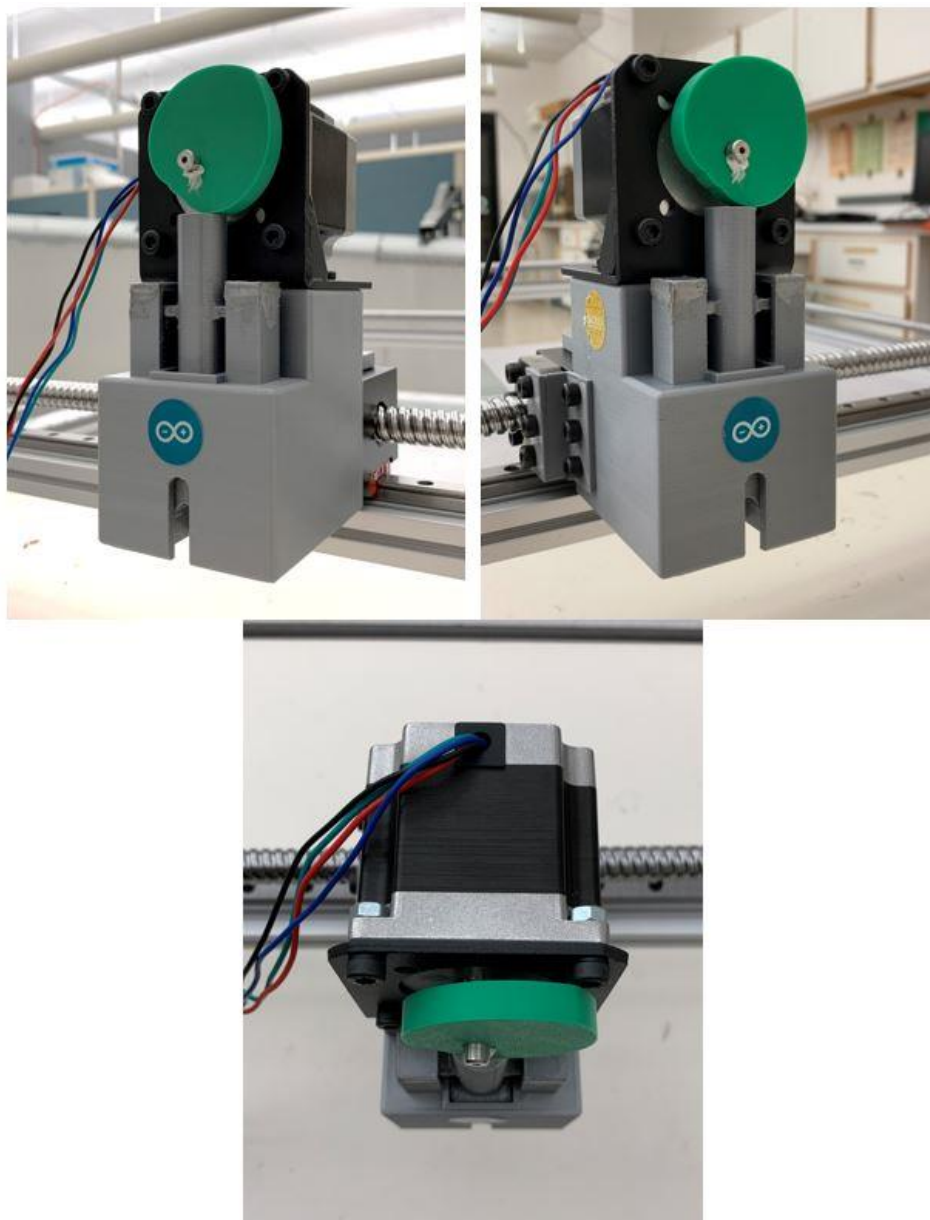


Figure 27. End-effector actuator system

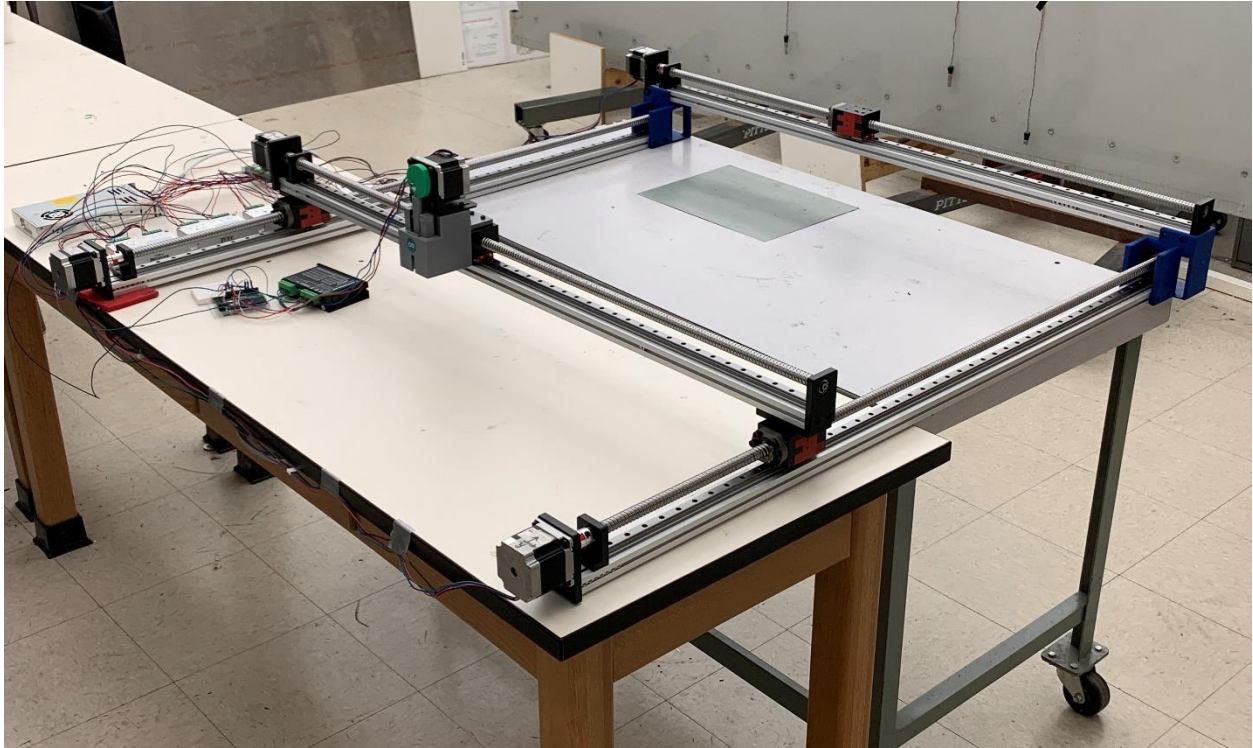


Figure 28. Isometric view of final assembly

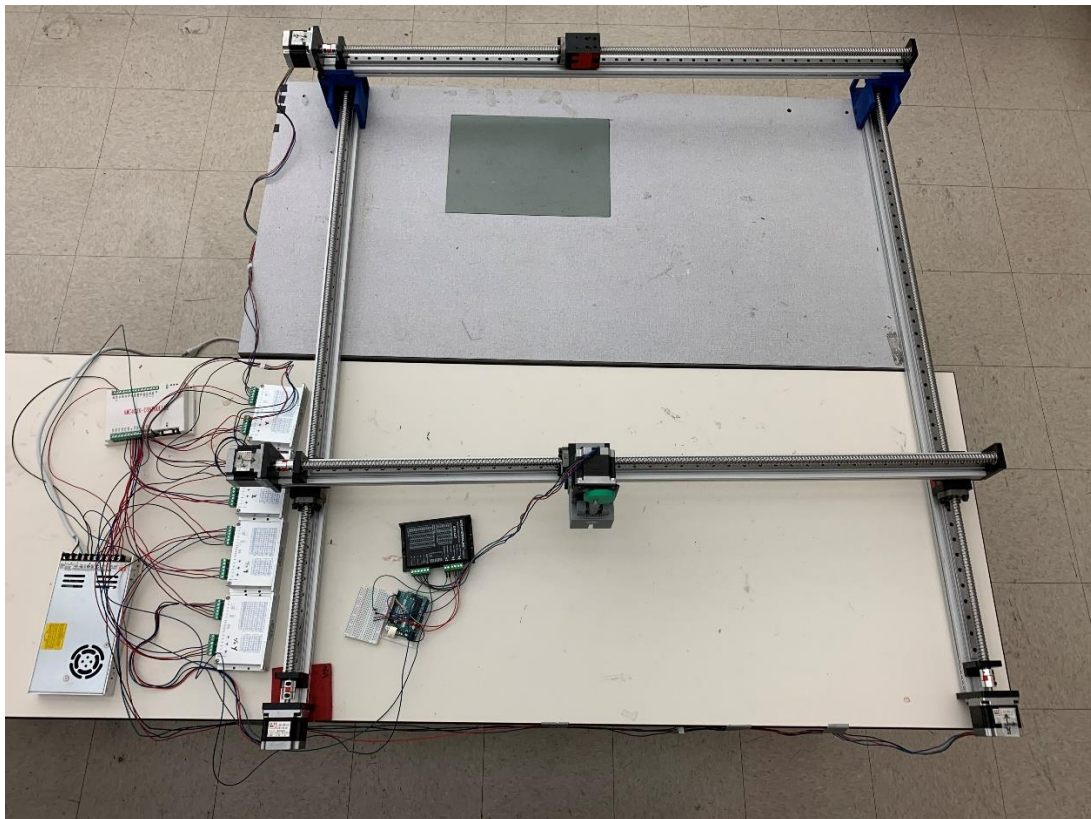


Figure 29. Top view of final assembly

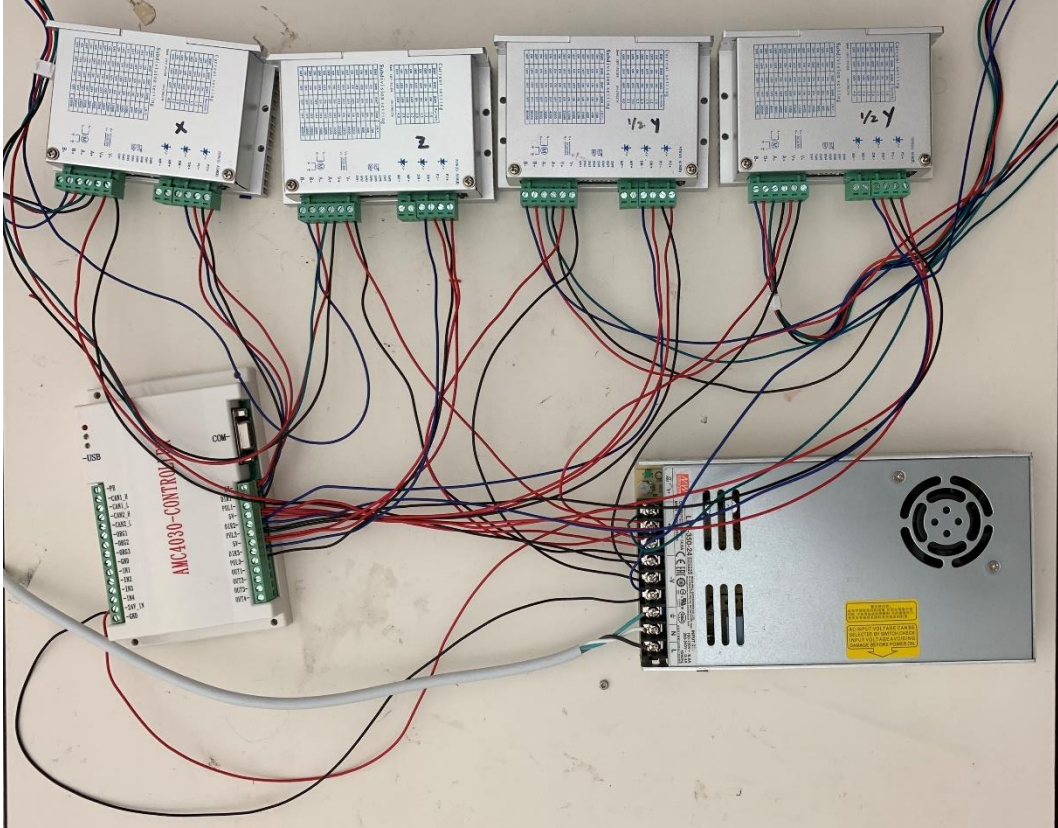


Figure 30. Wiring of linear guide system

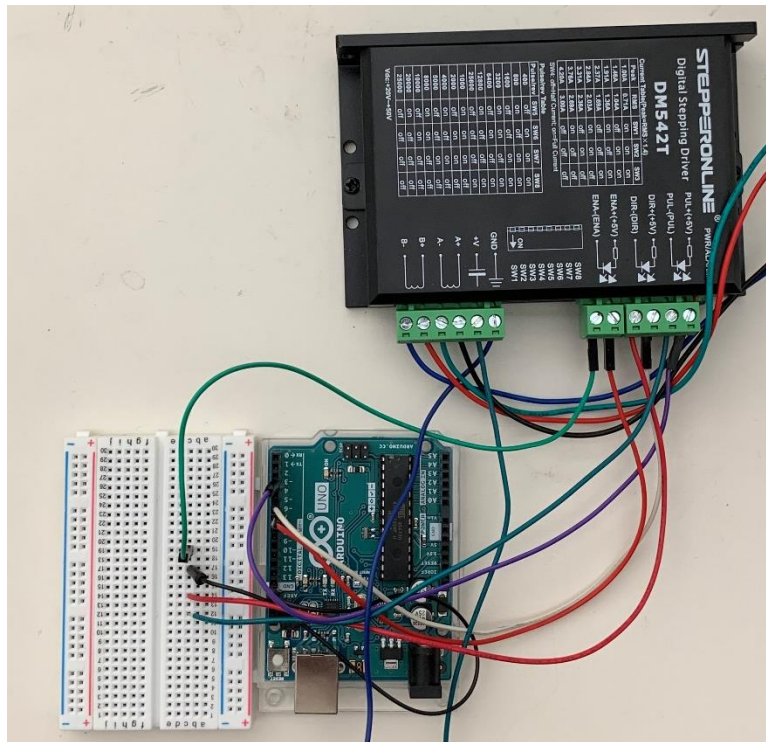


Figure 31. Wiring of end-effector actuator system

VI. Concluding Remarks

In this study, we have presented the design guidelines and final product of a Cartesian manipulation robot that can place ultrasonic transducers on test specimen for nondestructive evaluation experiments in the Material Degradation Laboratory at UCLA. The system can quickly and accurately move and place the transducers, then apply uniform pressure on the top surface for reliable transmission of ultrasonic waves. We also developed a software that allows the user to fully automate the experimental process and minimize human supervision. The future work includes better wire management of both sub-systems and nondestructive evaluation experiments where a large number of data points are taken.

References

- [1] L. Wang, F. Gao, Y. Zhang, L. Araque, S. Tai, B. Patel and A. Mal, "An Improved Damage Index for Nondestructive Evaluation of a Disbond in Honeycomb Sandwich Structure Using Guided Waves," *ASME Journal of Nondestructive Evaluation*, vol. 3, no. 3, p. 6, 2020.
- [2] G. Campbell and R. Lahey, "A survey of serious aircraft accidents involving fatigue fracture," *Elsevier International Journal of Fatigue*, vol. 6, no. 1, pp. 25-30, 1984.
- [3] H. Fujii, A. Yamashita and H. Asama, "Defect detection with estimation of material condition using ensemble learning for hammering test," in *IEEE International Conference on Robotics and Automation (ICRA)*, Stockholm, 2016.
- [4] J. Collins, "The Role of Failure Prevention Analysis in Mechanical Design," in *Failure of materials in mechanical design*, John Wiley & Sons, 1993, pp. 2-4.
- [5] J. Wang and C. Luo, "Automatic Wall Defect Detection Using an Autonomous Robot: A Focus on Data Collection," in *ASCE International Conference on Computing in Civil Engineering*, Atlanta, 2019.
- [6] B. Siciliano, L. Sciavicco, G. Oriolo and L. Villani, "Introduction," in *Robotics: Modelling, Planning and Control*, London, Springer, 2009, pp. 5-6.
- [7] J. J. Craig, "Introduction," in *Introduction to Robotics Mechanics and Control*, Pearson/Prentice Hall, 2005, pp. 4-7.
- [8] Y. Murakami, "Stress Concentration," in *Metal Fatigue*, Elsevier, 2019, pp. 13-27.
- [9] R. L. Norton, "Introduction," in *Cam Design and Manufacturing Handbook*, New York, Industrial Press, 2009, pp. 6-7.
- [10] FUYU, "High Precision Ball Screw Linear Motion Guide," [Online]. Available: <https://www.fuyumotion.com/high-precision-ball-screw-linear-motion-guide.html>. [Accessed 25 May 2020].
- [11] H. A. Rothbart, "Basic Curves," in *Cam Design Handbook*, McGraw-Hill, 2004, p. 33.
- [12] W. Pawlak, "Wear and coefficient of friction of PLA - Graphite composite in 3D printing technology," in *International Conference Engineering Mechanics*, Svatka, Czech Republic, 2018.